arXiv:hep-ph/0105238v1 22 May 2001

IFUSP/P-1475
UH-511-986-01

Probing Anomalous Quartic Couplings in $e\gamma$ and $\gamma\gamma$ Colliders

O. J. P. Éboli[1*] and J. K. Mizukoshi[2,†]
[1] *Instituto de Física, Universidade de São Paulo*
C.P. 66318, 05315–970, São Paulo, Brazil.
[2] *Department of Physics & Astronomy, University of Hawaii*
Honolulu, HI 96822, USA.

Abstract

We analyze the potential of the e^+e^- Linear Colliders, operating in the $e\gamma$ and $\gamma\gamma$ modes, to probe anomalous quartic vector–boson interactions through the multiple production of W's and Z's. We examine all $SU(2)_L \otimes U(1)_Y$ chiral operators of order p^4 that lead to new four–gauge–boson interactions but do not alter trilinear vertices. We show that the $e\gamma$ and $\gamma\gamma$ modes are able not only to establish the existence of a strongly interacting symmetry breaking sector but also to probe for anomalous quartic couplings of the order of 10^{-2} at 90% CL. Moreover, the information gathered in the $e\gamma$ mode can be used to reduced the ambiguities of the e^+e^- mode.

I. INTRODUCTION

The $SU_L(2) \times U_Y(1)$ local gauge symmetry of the Standard Model (SM) determines completely the triple and quartic vector–boson interactions. Therefore, the direct study of these couplings can further confirm the SM or give some hint on the existence of new phenomena at a higher scale. Moreover, it is important to independently measure the trilinear and quartic gauge boson couplings because there are extensions and limits of the SM [1] that leave the trilinear couplings unchanged but do modify the quartic vertices. Presently, the triple gauge–boson couplings are being probed at the Tevatron [2] and LEP [3] through the production of vector boson pairs, however, we have only started to study directly the quartic gauge–boson couplings [4,5]. Due to the limited available center–of–mass energy, the first quartic couplings to be studied contain two photons, and just at the CERN Large Hadron Collider (LHC) and the next generation of e^+e^- Linear Colliders (LC) we will be able to probe $VVVV$ ($V = W$ or Z) vertices.

*Email: eboli@fma.if.usp.br; † Email: mizuka@phys.hawaii.edu

If the $SU(2)_L \otimes U(1)_Y$ symmetry of the model is to be linearly realized, studies of the triple gauge–boson couplings will be able to furnish information on the gauge–boson four–point functions provided that dimension 8 and higher anomalous operators are suppressed. This is the case when the breaking of the $SU(2)_L \otimes U(1)_Y$ symmetry takes place via the Higgs mechanism with a relatively light elementary Higgs boson. If, on the other hand, no fundamental light Higgs particle is present in the theory, one is led to consider the most general effective Lagrangian which employs a nonlinear representation of the broken $SU(2)_L \otimes U(1)_Y$ gauge symmetry [6]. In this case the SM relation between the structure of the three– and four–point functions of the gauge bosons does not hold already at p^4 order, leaving open the question of the structure of the quartic vector–boson interactions.

LC provides a unique possibility to study $e\gamma$ and $\gamma\gamma$ collisions since high energy photons can be produced by laser backscattering [7]. These new modes of operation of the LC allow us to probe the $W^+W^-W^+W^-$ and W^+W^-ZZ couplings through the reactions

$$e^-\gamma \to W^-W^+W^-\nu_e \ , \tag{1}$$
$$e^-\gamma \to W^-ZZ\nu_e \ , \tag{2}$$
$$\gamma\gamma \to W^-W^+W^-W^+ \ , \tag{3}$$
$$\gamma\gamma \to W^-W^+ZZ \ , \tag{4}$$

which take place via weak boson fusion at high energies [8]. In this work, we access the reach of the LC operating in the $e\gamma$ and $\gamma\gamma$ modes to study the symmetry breaking sector via the measurement of quartic gauge couplings. We work in the framework of chiral Lagrangians, and we analyze all p^4 operators that lead to genuine quartic gauge interactions, *i.e.* these operators do not give rise to triple gauge–boson vertices, and consequently are not bounded by the study of the production of gauge–boson pairs. We also take into account realistic cuts, detection efficiencies and potential backgrounds.

At present the only information on quartic couplings $WWWW$ and $WWZZ$ is obtained indirectly as they modify the gauge–boson two–point functions at one loop [9]. The precise electroweak measurements both at low energy and at the Z pole, constrain the quartic anomalous couplings to be smaller than 10^{-3}–10^{-1} depending on the coupling. In the future, quartic interactions can be studied at the LHC through the reaction $pp \to VVX$ [10] while the following processes can give information on these couplings at the LC: $e^+e^- \to VVV$ [11], $e^+e^- \to FFVV$ [12], $e\gamma \to VVF$ [13], $\gamma\gamma \to VV$ [14], and $\gamma\gamma \to VVV$ [15], where $V = Z$, $W^\pm$ or γ and $F = e$ or ν_e.

In this work, we show that the LC operating in the $e\gamma$ or $\gamma\gamma$ modes not only can establish the existence of a strongly interacting symmetry breaking sector but also can lead to bounds on genuine quartic interactions of the order of 10^{-2} which turn out to be of the same order of magnitude of the attainable limits at the LHC and e^+e^- LC. Furthermore, the information gathered in the $e\gamma$ mode can be used to reduced the ambiguities of the e^+e^- mode, which exhibits two allowed regions, leading to a better determination of the quartic couplings.

The outline of this work is as follows. In Sec. II we present the chiral lagrangian formalism that we employed. We describe the calculational tools used in Sec. III, while the main features of the signal and backgrounds are discussed in Sec. IV. We present our results in Sec. V which also contains our conclusions.

II. THEORETICAL FRAMEWORK

If the electroweak symmetry breaking is due to a heavy (strongly interacting) Higgs boson, which can be effectively removed from the physical low–energy spectrum, or to no fundamental Higgs scalar at all, one is led to consider the most general effective Lagrangian which employs a nonlinear representation of the broken $SU(2)_L \otimes U(1)_Y$ gauge symmetry [6]. The resulting chiral Lagrangian is a non–renormalizable non–linear σ model coupled in a gauge–invariant way to the Yang–Mills theory. This model independent approach incorporates by construction the low-energy theorems [16], that predict the leading behavior of Goldstone boson amplitudes irrespective of the details of the symmetry breaking mechanism. Notwithstanding, unitarity implies that this low–energy effective theory should be valid up to some energy scale smaller than $4\pi v \simeq 3$ TeV [17], where new physics would come into play.

To specify the effective Lagrangian one must first fix the symmetry breaking pattern. We consider that the system presents a global $SU(2)_L \otimes SU(2)_R$ symmetry that is broken to $SU(2)_C$. With this choice, the building block of the chiral Lagrangian, in the notation of Ref. [6], is the dimensionless unimodular matrix field $\Sigma(x)$, which transforms under $SU(2)_L \otimes SU(2)_R$ as $(2,2)$:

$$\Sigma(x) \;=\; \exp\left(i\frac{\varphi^a(x)\tau^a}{v}\right) \,. \tag{5}$$

The φ^a fields are the would-be Goldstone fields and τ^a ($a = 1,\ 2,\ 3$) are the Pauli matrices. The $SU(2)_L \otimes U(1)_Y$ covariant derivative of Σ is defined as

$$D_\mu\Sigma \;\equiv\; \partial_\mu\Sigma + ig\frac{\tau^a}{2}W^a_\mu\Sigma - ig'\Sigma\frac{\tau^3}{2}B_\mu \,. \tag{6}$$

The lowest-order terms in the derivative expansion of the effective Lagrangian are

$$\mathcal{L}^{(2)} = \frac{v^2}{4}\mathrm{Tr}\left[\left(D_\mu\Sigma\right)^\dagger\left(D^\mu\Sigma\right)\right] + \beta_1 g'^2\frac{v^2}{4}\left(\mathrm{Tr}\left[TV_\mu\right]\right)^2 \,. \tag{7}$$

where we have introduced the auxiliary quantities $T \equiv \Sigma\tau^3\Sigma^\dagger$ and $V_\mu \equiv \left(D_\mu\Sigma\right)\Sigma^\dagger$ which are $SU(2)_L$–covariant and $U(1)_Y$–invariant. Notice that T is not invariant under $SU(2)_C$ custodial due to the presence of τ^3.

The first term in Eq. (7) is responsible for giving mass to the $W^\pm$ and Z gauge bosons for $v = (\sqrt{2}G_F)^{-1}$. The second term violates the custodial $SU(2)_C$ symmetry and contributes to $\Delta\rho$ at tree level, being strongly constrained by the low–energy data. This term can be understood as the low-energy remnant of a high–energy custodial symmetry breaking physics, which has been integrated out above a certain scale Λ. Moreover, at the one–loop level, this term is also required in order to cancel the divergences in $\Delta\rho$, arising from diagrams containing a hypercharge boson in the loop. This subtraction renders $\Delta\rho$ finite, although dependent on the renormalization scale [6].

At the next order in the derivative expansion, $D = 4$, several operators can be written down [6]. We shall restrict ourselves to those containing genuine quartic vector-boson interactions, which are

$$\mathcal{L}_4^{(4)} = \alpha_4 \left[\mathrm{Tr}\left(V_\mu V_\nu\right)\right]^2 \ , \tag{8}$$

$$\mathcal{L}_5^{(4)} = \alpha_5 \left[\mathrm{Tr}\left(V_\mu V^\mu\right)\right]^2 \ , \tag{9}$$

$$\mathcal{L}_6^{(4)} = \alpha_6 \ \mathrm{Tr}\left(V_\mu V_\nu\right) \mathrm{Tr}\left(TV^\mu\right) \mathrm{Tr}\left(TV^\nu\right) \ , \tag{10}$$

$$\mathcal{L}_7^{(4)} = \alpha_7 \ \mathrm{Tr}\left(V_\mu V^\mu\right) \left[\mathrm{Tr}\left(TV^\nu\right)\right]^2 \ , \tag{11}$$

$$\mathcal{L}_{10}^{(4)} = \frac{1}{2}\alpha_{10} \left[\mathrm{Tr}\left(TV_\mu\right) \ \mathrm{Tr}\left(TV_\nu\right)\right]^2 \ . \tag{12}$$

In an arbitrary gauge, these Lagrangian densities lead to quartic vertices involving gauge bosons and/or Goldstone bosons. In the unitary gauge, these effective operators give rise to anomalous $ZZZZ$ (all operators), W^+W^-ZZ (all operators except $\mathcal{L}_{10}^{(4)}$), and $W^+W^-W^+W^-$ ($\mathcal{L}_4^{(4)}$ and $\mathcal{L}_5^{(4)}$) interactions. Moreover, the interaction Lagrangians $\mathcal{L}_6^{(4)}$, $\mathcal{L}_7^{(4)}$, and $\mathcal{L}_{10}^{(4)}$ violate the $SU(2)_C$ custodial symmetry due to the presence of T in their definitions. Notice that quartic couplings involving photons remain untouched by the genuine quartic anomalous interactions at the order $D = 4$. The Feynman rules for the quartic couplings generated by these operators can be found in the last article of Ref. [6].

In chiral perturbation theory, the p^4 contributions to the processes (1)–(4) arise from the tree level insertion of p^4 operators, as well as from one-loop corrections due to the p^2 interactions, which renormalize the p^4 operators [6]. However, the loop corrections to the scattering amplitudes are negligible in comparison to the p^4 contributions for the range of values of the couplings and center–of–mass energies considered in this paper. Therefore, numerically, our analysis is consistent even though we neglected the loop corrections and kept only the tree–level p^4 contributions.

In the effective–W approximation [8,18], the signals (1)–(4) are described by the scattering $V_LV_L \to V_LV_L$. These processes, however, do not respect the unitarity of the partial–wave amplitudes (a_ℓ^I) at large subprocess center–of–mass energies M_{VV} [17,19,20]. Therefore, the chiral expansion is valid only for values of M_{VV} and α_i such that $|a_\ell^I| \lesssim 1/2$. For higher VV invariant masses, rescattering effects are important to unitarize the amplitudes. Taking into account this fact, we conservatively restricted our analyses to invariant masses $M_{VV} < 1.25$ TeV. This requirement corresponds to a sharp–cutoff unitarization [21].

III. CALCULATIONAL TOOLS

In order to study the quartic couplings of vector bosons we analyzed the processes (1)–(4) which may receive contributions from anomalous $WWZZ$ and $ZZZZ$ interactions. The signal for vector boson fusion in the $\gamma\gamma$ ($e\gamma$) reactions is characterized by the presence of two central vector bosons as well as by two (one) extra ones in the forward and backward regions of the detector, which can be used to tag the events. Therefore, we ordered the produced vector bosons according to their rapidities and assumed that the strongly scattered ones have smaller rapidities in absolute value.

The signal and backgrounds were simulated at the parton level with full tree level matrix elements. We include in our calculations all SM and anomalous contributions that lead to the final states (1)–(4) , taking into account the effect of interferences between the anomalous and SM amplitudes. This was accomplished by numerically evaluating helicity amplitudes for all subprocesses using MADGRAPH [22] in the framework of HELAS [23], with the anomalous

couplings arising from the Lagrangians (8)–(12) being implemented as additional Fortran routines. For the sake of illustration, the SM background for the processes (1) to (4) requires the evaluation of 87, 54, 240, and 74 Feynman diagrams respectively.

In our calculations we included the reconstruction efficiency for central W's and Z's which are required to have $|\eta_{W(Z)}| < 1$. Using the results of Ref. [24], we assumed that reconstruction efficiency of a W (Z) is 85% (74%) while the probability for misidentifying a Z as a W (a W as a Z) being 22% (10%). We studied the probability of tagging forward W's and Z's with $1.5 < |\eta_{W(Z)}| < 3$ by consistently including their decay into jets. Our analysis showed that just one of the jets coming from a vector boson in the above rapidity region has $|\eta_j| < 2$ and that the tagging efficiency of the spectator W from the presence of this jet is 40%.

The most promising mechanism to generate hard photon beams in an e^+e^- linear collider is laser backscattering, which can lead to a rich source of $e\gamma$ and $\gamma\gamma$ interactions with essentially the same luminosity and center-of-mass energy of the parent e^+e^- collider [7]. We verified that the polarization of the beams do not change significantly our results, therefore, we present our results for unpolarized electron and laser beams for the sake of simplicity. In this case, the backscattered photon distribution function [25] is

$$F_{\gamma/e}(x,\xi) \equiv \frac{1}{\sigma_c}\frac{d\sigma_c}{dx} = \frac{1}{D(\xi)}\left[1 - x + \frac{1}{1-x} - \frac{4x}{\xi(1-x)} + \frac{4x^2}{\xi^2(1-x)^2}\right] , \tag{13}$$

with

$$D(\xi) = \left(1 - \frac{4}{\xi} - \frac{8}{\xi^2}\right)\ln(1+\xi) + \frac{1}{2} + \frac{8}{\xi} - \frac{1}{2(1+\xi)^2} , \tag{14}$$

where σ_c is the Compton cross section, $\xi \simeq 4E\omega_0/m_e^2$, m_e and E are the electron mass and energy respectively, and ω_0 is the laser-photon energy. The quantity x stands for the ratio between the scattered photon and initial electron energy and its maximum value is

$$x_{\rm max} = \frac{\xi}{1+\xi} . \tag{15}$$

In what follows, we assumed that the laser frequency is such that $\xi = 2(1+\sqrt{2})$, which leads to the hardest possible spectrum of photons with a large luminosity since the creation of soft e^+e^- pairs in hard γ–laser interaction is avoided with this choice. In this case, $x_{\rm max} \simeq 0.83$.

The cross section for $\gamma\gamma$ fusion processes can be obtained by folding the elementary cross section for the $\gamma\gamma$ subprocesses with the photon distributions, *i.e.*,

$$d\sigma(e^+e^- \to \gamma\gamma \to X)(s) = \int dx_1 dx_2 \; F_{\gamma/e}(x_1,\xi)\; F_{\gamma/e}(x_2,\xi)\; d\hat{\sigma}(\gamma\gamma \to X)(\hat{s}) , \tag{16}$$

where $\sqrt{s}$ ($\sqrt{\hat{s}}$) is the e^+e^- ($\gamma\gamma$) center-of-mass energy. In the case of $e\gamma$ collisions we should drop one of the integrals on the photon spectrum. In our analyses we considered two e^+e^- center–of–mass energies $\sqrt{s} = 2$ and 3 TeV which leads to a maximum $\gamma\gamma$ ($e\gamma$) center–of–mass energy of 1.7 and 2.5 (1.8 and 2.7) TeV respectively. We assumed that the integrated luminosity for the parent e^+e^- machine is 500 fb^{-1} which is a conservative choice since we can always tune up the beam shape in order to boost the $\gamma\gamma$ and $e\gamma$ luminosities [7].

IV. SIGNAL AND BACKGROUND PROPERTIES

Strongly interacting symmetry breaking sectors (SEWS) modify the dynamics of longitudinal vector bosons. However, it is impossible to determine the polarization of vector bosons on an event–by–event basis, and consequently, we have to work harder to extract the SEWS signal. Taking into account that the electroweak production of transversely polarized vector bosons in the SM is approximately independent of the Higgs boson mass, and that the $V_L V_L$ production is small for light Higgs bosons [26], we define the signal for SEWS as an excess of events in the VV scattering channels with respect to the SM with a light Higgs, *i.e.*

$$\sigma_{\rm signal} \equiv \sigma(\alpha_i) - \sigma_{\rm sm}^{\rm lh} \quad , \tag{17}$$

where $\sigma_{\rm sm}^{\rm lh} = \sigma_{\rm sm}\Big|_{M_H=100\ {\rm GeV}}$ and we sum over the vector-boson polarizations. In principle, we can have a signal even for $\alpha_i \equiv 0$, indicating the existence of SEWS, since there is no Higgs in our model to cut off the growth of the scattering amplitudes. In this case that it is possible to establish the existence of SEWS, we should verify whether the anomalous couplings α_i are compatible with zero or not. In this scenario we define the $\sigma_{\rm signal}$ with respect to vanishing α's, *i.e.*

$$\sigma_{\rm signal} \equiv \sigma(\alpha_i) - \sigma(0) \ . \tag{18}$$

The most general expression for the total cross sections of the processes (1)–(4) can be written as

$$\sigma \equiv \sigma_{\rm sm}^{hh} + \alpha_j \ \sigma_{\rm int}^{\alpha_j} + \alpha_i \alpha_j \ \sigma_{\rm ano}^{\alpha_i \alpha_j} \ , \tag{19}$$

where $\sigma_{\rm sm}^{hh}$, $\sigma_{\rm int}^{\alpha_j}$, and $\sigma_{\rm ano}^{\alpha_i \alpha_j}$ are, respectively, the SM cross section without the inclusion of the Higgs boson effects, interference between the heavy Higgs SM and the anomalous contributions and the pure anomalous cross section. α_i stands for any of the anomalous quartic couplings appearing in Eqs. (8)–(12).

One of the important features of the vector boson scattering is the presence of vector bosons at large rapidities which can be used to tag the events. In our analyses we required the existence of spectator vector bosons with

$$1.5 < |\eta_{W(Z)}| < 3 \ , \tag{20}$$

which lead to a detectable spectator jet 40% of the time. Since, we detect only one of the jets coming from forward W's and Z's, there is one additional background due to the production of top quark pairs when the b from the top decay is taken as the tagging forward jet. Therefore we vetoed these events tagging b jets, assuming a b tagging efficiency of 60%. Moreover, we assume a probability of 5% that a light-quark jet is mistagged as a b–quark jet.

A. $e\gamma$ mode

In order to suppress the backgrounds and enhance the signal for the anomalous quartic interactions in processes (1) and (2) we applied the following set of cuts:

(*i*) We required the tagging of a large rapidity vector boson as described above.

(*ii*) We vetoed events presenting b tagged jets in order to reduce the top production background.

(*iii*) We demanded the presence of a pair W^+W^- (ZZ) in the process $e\gamma \to W^-W^+W^-\nu_e$ ($W^-ZZ\nu_e$) with $p_T^{W(Z)} > 200$ GeV and $|\eta_{W(Z)}| < 1$. In order to access the relevance of this p_T cut see Fig. 1.

(*iv*) We also required the invariant mass of the vector boson pair to be in the range $0.5 < M_{VV} < 1.25$ TeV. The upper limit of this cut is quite important since it prevents the effective operators (8)–(12) to be used in a energy regime where unitarity is violated and rescattering effects become important. The lower limit of this cut aims to reduce the backgrounds; see Fig. 2.

We display in Table I our results for the coefficients σ in Eq. (19) after applying the above cuts, however before taking into account the detection efficiencies. In the $W^-ZZ\nu_e$ production, the central gauge boson pair can be either W^-Z or ZZ, therefore, we show these two cases in Table I. As expected, the cross sections rise as the center–of–mass energy increases. Moreover, it is clear from this table that the $W^-W^+W^-\nu_e$ process not only leads to a larger statistics but also it is more sensitive to the quartic anomalous couplings. In order to obtain the signal cross section, we must fold the results in Table I with the reconstruction efficiencies and take into account the misidentification probabilities since both processes, $W^-W^+W^-\nu_e$ and $W^-ZZ\nu_e$, can lead to events WW + jet and ZZ + jet, where the pair of gauge bosons is central and the single jet comes from a forward W or Z. For instance, about 5% of the ZZ + jet signal events are due to vector boson misidentification in the reaction $WWW\nu_e$ for $\alpha_4 = \alpha_5 = 0$.

Table II contains the total light Higgs background cross section for processes (1) and (2) after cuts and detection efficiencies. We also display in this table the fraction F of the total background due to each reaction. Notice that the bulk of the background to the WW + jet events is due to the production of $WWW\nu$ in the scope of the SM. However, some fraction of the background ($\simeq 9\%$) to the ZZ + jet events is due to misidentification of W's generated by reaction (1). In $e\gamma$ production the $t\bar{t}$ background is not important.

B. $\gamma\gamma$ mode

The production of $W^-W^+W^-W^+$ and W^-ZZW^+ in $\gamma\gamma$ collisions due to anomalous quartic interactions can be enhanced using the same cuts employed in the $e\gamma$ case, with the exception that we now require the tagging of two forward W's. Table III contains our results for the parameters appearing in (19) after cuts but before introducing the detection efficiencies. In this mode, the $W^-W^+W^-W^+$ production not only possesses the highest cross section but also it exhibits a stronger dependence on the anomalous couplings. Analogously to the $e\gamma$ case, we have to conveniently introduce the detection efficiencies, branching ratios, and misidentification probabilities in order to obtain the expected number of events.

We show the total light Higgs backgrounds in the $\gamma\gamma$ mode and its composition in Table IV. The $WW+2$–jet signal events have as major backgrounds the production of longitudinal

$WWWW$ in the scope of the SM and the $t\bar{t}$ production, with a small contribution from the misidentification of vector bosons. It is interesting to notice that the top pair background represents almost half of the total background at 2 TeV with its importance decreasing at higher energies. For the $ZZ + 2$–jet events, the major background is the production of W^-ZZW^+ within the SM with $t\bar{t}$ production and the particle misidentification being responsible for 17–25% of the background events.

V. DISCUSSION AND CONCLUSIONS

Initially we studied whether an $e\gamma$ or $\gamma\gamma$ collider can unravel the existence of a symmetry breaking dynamics different from the one predicted by the SM. In order to do that we analyzed the reactions (1) to (4) assuming that the number of observed events is the one predict by the SM with a light Higgs boson. We display in Fig. 3a the 5σ allowed region in the $e\gamma$ mode for an e^+e^- center–of–mass energy of 2 TeV and an integrated luminosity of 500 fb^{-1}. As expected, most of WW + jet events are due to $W^-W^+W^-\nu_e$ production and this channel leads to more stringent limits and dominates the combined bounds. This figure clearly shows that the combined results for the WW + jet and ZZ + jet events will be able to establish the existence of a new dynamics in the symmetry breaking system since the agreement with experiment is only possible for non-vanishing quartic couplings. Fig. 3b contains the results for a $\gamma\gamma$ collider assuming the same center–of–mass energy, luminosity and confidence level. The $\gamma\gamma$ mode at 2 TeV will not be able to establish a departure from the SM, and we verified that the signal of new dynamics only appears at higher center–of–mass energies, *e.g.* 3 TeV. For the sake of comparison, we estimated that establishing the existence of SEWS in the LC e^+e^- mode will require an integrated luminosity of the order of 50 fb^{-1} for a center–of–mass energy of 1.6 TeV.

Having established the existence of a new dynamics we probed the LC capability to constrain anomalous quartic vector boson couplings by assuming that the number of observed events is the one predicted by the SM without the Higgs boson; see Eq. (18). We present in Fig. 4 the 90% CL bounds on the $SU(2)_C$ conserving quartic couplings coming from the reactions (1) and (2), assuming center–of–mass energies of 2 and 3 TeV and an integrated luminosity of 500 fb^{-1}. Here the best limits also come from the WW + jet production, however, the combined results are much more restrictive than this channel alone since the ZZ + jet allowed region has a different orientation than the WW + jet one. Moreover, the constraints improve by a factor of $\mathcal{O}(2)$ when the center–of–mass energy increases from 2 TeV to 3 TeV.

The bounds on the couplings α_4 and α_5 obtained in the $e\gamma$ mode of the LC are of the same order of the ones coming from the e^+e^- mode [12]. Moreover, the $e\gamma$ mode possesses only one allowed region in the plane (α_4, α_5), while the reactions $e^+e^- \to \bar{\nu}\nu W^+W^-$ and and $\bar{\nu}\nu ZZ$ lead to two allowed regions, one in the vicinity of $(0, 0)$ and the second one having only non-vanishing values of the anomalous couplings; see Ref. [12]. Therefore, the information gathered in the $e\gamma$ mode can be used to reduced the ambiguities of the e^+e^- mode, analogously to what happens in the e^-e^- mode [12].

Fig. 5 shows the attainable bounds on α_4 and α_5 through the reactions $\gamma\gamma \to WW + 2$ jets and $ZZ + 2$ jets for an integrated luminosity of 500 fb^{-1} and center–of–mass energies of 2 and 3 TeV. In this mode, the best limits originate from the $WW + 2$–jet events, which

receives most of contributions from $W^+W^-W^-W^+$, since this process exhibits the largest cross section. Moreover, the process $ZZ + 2$ jets turns out to be important to exclude a large fraction of the region allowed by the $WW + 2$ jet production. Like the $e\gamma$ mode, the $\gamma\gamma$ collider also gives rise to just one allowed region around the origin, therefore it is complementary to the e^+e^- mode too. However, the limits that can be obtained from this mode are weaker than the ones coming the the e^+e^- and $e\gamma$ modes.

Up to now we concentrated our analyses on the $SU(2)_C$ conserving quartic operators (8) and (9). First of all, the effective interaction (12) can not be constrained by any of the processes studied here since it leads only to a $ZZZZ$ vertex. The vertex W^+W^-ZZ associated to α_6 (α_7) is equal to the one generated by α_4 (α_5), however the operators (8) and (9) do not induce $WWWW$ interactions. Therefore, α_6 and α_7 do not contribute to the most stringent processes $e\gamma \to W^+W^-W^+\nu_e$ and $\gamma\gamma \to W^+W^-W^+W^-$. From this fact we expect that the bounds on these operators should be much weaker, analogously to what takes place in the e^+e^- mode. In Fig. 6 we display the combined limits on these operators for a 2 and 3 TeV LC.

In brief, the $e\gamma$ can help us to have a better understanding of the symmetry breaking sector of the electroweak interactions since it leads to constraints $\mathcal{O}(0.005)$ on the $SU(2)_C$ conserving quartic gauge boson interactions for a 2 TeV LC. Moreover, this mode is complementary to the e^+e^- one since it allow us to resolve the ambiguity that the last mode presents on the limits on these couplings. Analogously to the traditional e^+e^- mode the $e\gamma$ bounds on $SU(2)_C$ violating operators are also much less stringent. We also showed that the $\gamma\gamma$ mode is complementary to the e^+e^- one, however that mode leads to bounds that are a factor 5–10 weaker.

ACKNOWLEDGMENTS

This work was supported by Conselho Nacional de Desenvolvimento Científico e Tecnológico (CNPq), by Fundação de Amparo à Pesquisa do Estado de São Paulo (FAPESP), by Programa de Apoio a Núcleos de Excelência (PRONEX), and by the U. S. Department of Energy under contract number DE-FG03-94ER40833.

REFERENCES

[1] A. Hill and J. J. van der Bij, Phys. Rev. D**36**, 3463 (1987); R. Casalbuoni, *et al.*, Nucl. Phys. **B282**, 235 (1987); Phys. Lett. **B155**, 95 (1985); V. Borodulin and G. Jikia, Nucl. Phys. **B520**, 31 (1998); S. Godfrey, *Quartic Gauge Boson Couplings* in Proceedings of the International Symposium on Vector Boson Self-Interactions, edited by U. Baur, S. Errede, T. Muller (American Inst. Phys., 1996), p. 209 [hep-ph/9505252].

[2] K. Gounder, CDF Collaboration, hep-ex/9903038; B. Abbott *et al.*, DØ Collaboration, Phys. Rev. **D62**, 052005 (2000).

[3] R. Barate *et al.*, ALEPH Collaboration, Phys. Lett. **B462**, 389 (1999); CERN EP/2001-022 (hep-ex/0104034); P. Abreu *et al.*, DELPHI Collaboration, Phys. Lett. **B459**, 382 (1999); M. Acciarri *et al.*, L3 Collaboration, Phys. Lett. **B487**, 229 (2000); Phys. Lett. **B489**, 55 (2000); G. Abbiendi *et al.*, OPAL Collaboration, Eur. Phys. J. **C19**, 1 (2001).

[4] G. Abbiendi *et al.*, OPAL Collaboration, Phys. Lett. **B471**, 293 (1999); M. Acciarri *et al.*, L3 Collaboration, Phys. Lett. **B478**, 39 (2000); Phys. Lett. **B490**, 187 (2000).

[5] For recent results from the LEP four experiments combined, see http://lepewwg.web.cern.ch/LEPEWWG/lepww/tgc/.

[6] T. Appelquist and C. Bernard, Phys. Rev. **D22**, 200 (1980); A. Longhitano, Phys. Rev. **D22**, 1166 (1980); Nucl. Phys. **B188**, 118 (1981).

[7] See for instance, V. Telnov, report hep-ex/0003024 and references there in.

[8] K. Hagiwara, I. Watanabe, and P. M. Zerwas, Phys. Lett. **B278**, 187 (1992).

[9] A. Brunstein, O. J. P. Éboli, and M. C. Gonzalez-Garcia, Phys. Lett. **B375**, 233 (1996); S. Alam, S. Dawson, and R. Szalapski, Phys. Rev. **D57**, 1577 (1998)

[10] A. Dobado, D. Espriu, and M. J. Herrero, Z. Phys. **C50**, 205 (1991); J. Bagger, S. Dawson, and G. Valencia, Nucl. Phys. **B399**, 364 (1993); A. Dobado and M. T. Urdiales, FTUAM 94/29 (hep-ph/9502255); A. Dobado, M. J. Herrero, J. R. Peláez, E. Ruiz Morales, and M. T. Urdiales, Phys. Lett. **B352**, 400 (1995); A. S. Belyaev, *et al.*, Phys. Rev. **D59**, 015022 (1999); O. J. P. Éboli, M. C. Gonzalez Garcia, S. M. Lietti, and S. F. Novaes, Phys. Rev. **D63**, 075008 (2001).

[11] V. Barger and T. Han, Phys. Lett. **B212**, 117 (1988); V. Barger, T. Han, and R. J. N. Phillips, Phys. Rev. **D39**, 146 (1989); A. Tofighi-Niaki and J. F. Gunion, Phys. Rev. **D39**, 720 (1989); G. Bélanger and F. Boudjema, Phys. Lett. **B288**, 201 (1992); G. A. Leil and W. J. Stirling, J. Phys. **G21**, 517 (1995); O. Éboli, M. C. Gonzalez-Garcia, and J. K. Mizukoshi, Phys. Rev. **D58**, 034008 (1998); T. Han, H. He, and C. P. Yuan, Phys. Lett. **B422**, 294 (1998).

[12] E. Boos *et al.*, Phys. Rev. **D57**, 1553 (1998); Phys. Rev. **D61**, 077901 (2000).

[13] O. J. P. Éboli, M. C. Gonzalez-Garcia, and S. F. Novaes, Nucl. Phys. **B411**, 381 (1994).

[14] G. Bélanger and F. Boudjema, Phys. Lett. **B288**, 210 (1992).

[15] O. J. P. Éboli, M. B. Magro, P. G. Mercadante, and S. F. Novaes, Phys. Rev. **D52**, 15 (1995).

[16] M. S. Chanowitz, M. Golden, and H. Georgi, Phys. Rev. **D36**, 1490 (1987).

[17] B. W. Lee, C. Quigg, and H. B. Thacker, Phys. Rev. **D16**, 1519 (1977).

[18] G. L. Kane, W. W. Repko, and W. B. Rolnick, Phys. Lett. **148B**, 367 (1984); S. Dawson, Nucl. Phys. **B249**, 42 (1985).

[19] B. W. Lee, C. Quigg, and H. B. Thacker, Phys. Rev. Lett. **38**, 883 (1977); D. Dicus and V. Mathur, Phys. Rev. **D7**, 3111 (1973).

[20] J. M. Cornwall, D. N. Levin, and G. Tiktopoulos, Phys. Rev. **D10**, 1145 (1974); C. E. Vayonakis, Lett. Nuovo Cim. **17**, 383 (1976); M. S. Chanowitz and M. K. Gaillard, Nucl. Phys. **B261**, 379 (1985).
[21] V. Barger *et al.*, Phys. Rev. **D42**, 3052 (1990).
[22] W. Long and T. Stelzer, Comput. Phys. Commun. **81**, 357 (1994).
[23] H. Murayama, I. Watanabe and K. Hagiwara, KEK report 91-11 (unpublished).
[24] V. Barger *et al.*, Phys. Rev. **D52**, 3815 (1995).
[25] I. F. Ginzburg, G. L. Kotkin, V. G. Serbo, and V. I. Telnov, Nucl. Instrum. Methods **205**, 47 (1983); **219**, 5 (1984); V. I. Telnov, Nucl. Instrum. Methods **A294**, 72 (1990).
[26] J. Bagger, *et al.* Phys. Rev. **D49**, 1246 (1994); *idem* Phys. Rev. **D52**, 3878 (1995).

TABLES

reaction	$\sqrt{s_{ee}}$ TeV	$\sigma_{\rm sm}^{hh}$ (fb)	$\sigma_{\rm int}^{\alpha_4}$ (fb)	$\sigma_{\rm ano}^{\alpha_4\alpha_4}$ (fb)	$\sigma_{\rm int}^{\alpha_5}$ (fb)	$\sigma_{\rm ano}^{\alpha_5\alpha_5}$ (fb)	$\sigma_{\rm ano}^{\alpha_4\alpha_5}$ (fb)
$W^-[W^+W^-]\nu_e$	2	4.84	-74.3	19500.	31.0	21500.	34900.
$W^-[W^+W^-]\nu_e$	3	10.3	-319.	121×10^3	99.	133×10^3	221×10^3
$W^-[ZZ]\nu_e$	2	1.07	24.4	404.	67.6	2716	1901
$W^-[ZZ]\nu_e$	3	2.83	95.9	2030	258.	12600.	8930.
$[W^-Z]Z\nu_e$	2	0.256	3.82	128.	8.26	383.	248.
$[W^-Z]Z\nu_e$	3	0.38	9.25	747.	15.0	977.	63.0

TABLE I. Values for the standard model, pure anomalous and interference cross sections after cuts, according to Eq. (19), for $e\gamma \to W^-W^+W^-\nu_e$ and $W^-ZZ\nu_e$ and several e^+e^- center–of–mass energies. We display between brackets the vector bosons produced in the central region.

events	$\sqrt{s_{ee}}$ TeV	$\sigma_{\rm sm}^{lh}$ (fb)	$F(WWW\nu)$	$F(W[ZZ]\nu)$	$F(Z[WZ]\nu)$	$F(t\bar{t})$
WW + jet	2	0.480	96.2%	1.0%	1.5%	1.2%
WW + jet	3	0.879	96.9%	1.2%	1.1%	0.7%
ZZ + jet	2	6.5×10^{-2}	9.2%	86.5%	4.6%	0.0%
ZZ + jet	3	0.139	8.6%	88.5%	2.9%	0.0%

TABLE II. Total light Higgs background cross section in the $e\gamma$ mode after cuts and detection efficiencies as well as its composition. We display between brackets the vector bosons produced or identified in the central region.

reaction	$\sqrt{s_{ee}}$ TeV	$\sigma_{\rm sm}^{hh}$ (fb)	$\sigma_{\rm int}^{\alpha_4}$ (fb)	$\sigma_{\rm ano}^{\alpha_4\alpha_4}$ (fb)	$\sigma_{\rm int}^{\alpha_5}$ (fb)	$\sigma_{\rm ano}^{\alpha_5\alpha_5}$ (fb)	$\sigma_{\rm ano}^{\alpha_4\alpha_5}$ (fb)
$W^-[W^+W^-]W^+$	2	4.27	-45.9	6450.	-25.4	8920.	13400.
$W^-[W^+W^-]W^+$	3	11.9	-354.	89000.	-224.	124×10^3	186×10^3
$W^-[ZZ]W^+$	2	0.787	8.81	129.	31.0	771.	522.
$W^-[ZZ]W^+$	3	2.77	68.4	1530.	235.	8390.	5650.
$[W^\pm Z]ZW^\mp$	2	0.596	2.88	98.2	8.46	263.	117.
$[W^\pm Z]ZW^\mp$	3	1.17	11.2	1100.	31.3	1630.	-240.

TABLE III. Values for the standard model, pure anomalous and interference cross sections after cuts, according to Eq. (19), for $\gamma\gamma \to W^-W^+W^-W^+$ and W^-ZZW^+ and several e^+e^- center–of–mass energies. We display between brackets the vector bosons produced in the central region.

events	$\sqrt{s_{ee}}$ TeV	$\sigma^{lh}_{\rm sm}$ (fb)	$F(WWWW)$	$F(W[ZZ]W)$	$F([WZ]ZW)$	$F([WW]ZZ)$	$F(t\bar{t})$
WW + 2 jets	2	0.34	50.4%	0.6%	2.1%	0.9%	46.0%
WW + 2 jets	3	0.51	80.2%	1.0%	2.5%	0.8%	15.5%
ZZ + 2 jets	2	0.028	7.1%	75.0%	10.7%	0.1%	7.1%
ZZ + 2 jets	3	0.071	8.4%	82.5%	7.0%	0.7%	1.4%

TABLE IV. Total light Higgs background cross section in the $\gamma\gamma$ mode after cuts and detection efficiencies and its composition. We display between brackets the vector bosons produced in the central region.

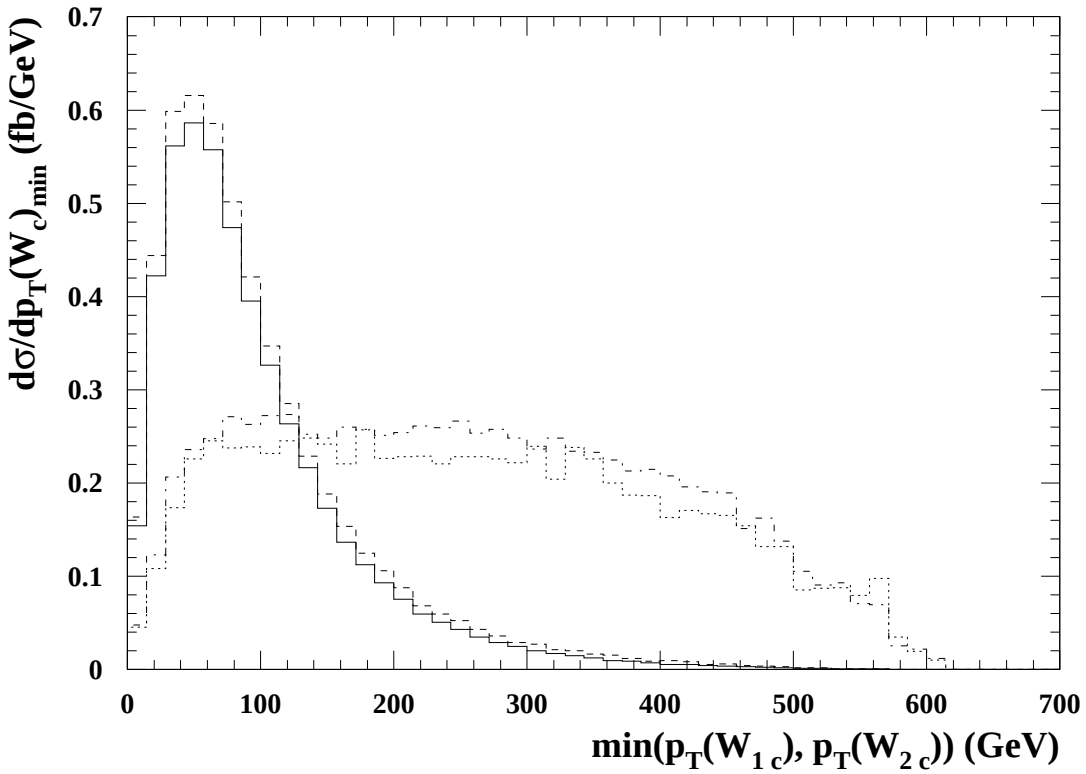

FIG. 1. Minimal transverse momentum of the central W bosons for the process $e^+e^- \to e^-\gamma \to W^-W^+W^-\nu_e$ at $\sqrt{s_{ee}} = 2$ TeV. The solid (dashed) line stands for the SM with a light Higgs (heavy Higgs) and the dotted (dotted-dashed) is the anomalous contribution for $\alpha_{4(5)} = 0.05$.

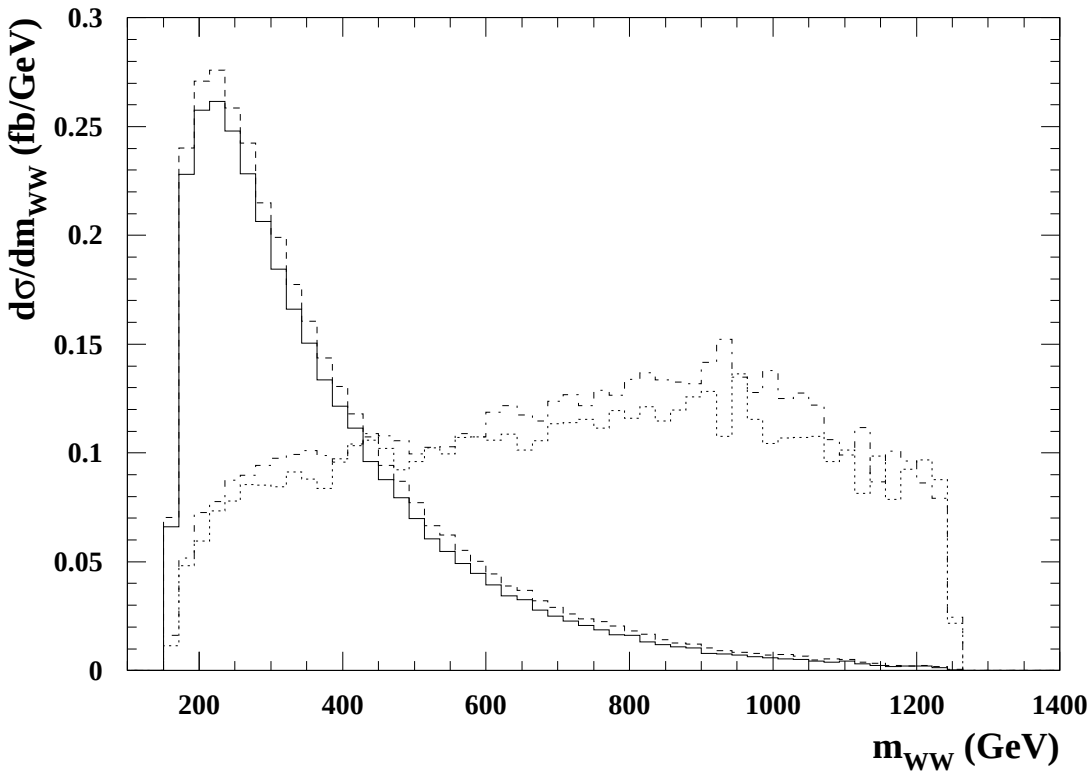

FIG. 2. Invariant mass distribution of the central W boson pair for the process $e^+e^- \to e^-\gamma \to W^-W^+W^-\nu_e$ at $\sqrt{s_{ee}} = 2$ TeV. We applied the regularization cut $m_{WW} < 1.25$ TeV and employed the conventions as in Fig. 1.

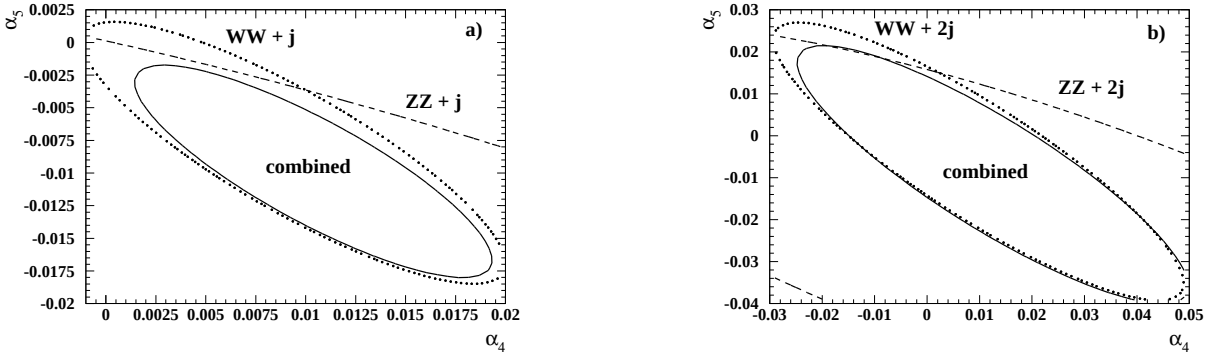

FIG. 3. 5σ allowed region in the (α_4, α_5) plane assuming that we observed the expected number of events predict by the SM with a light Higgs boson in the WW + jet (dots), ZZ + jet (dashes), and combined reactions (solid). We assumed a e^+e^- center–of–mass energy of 2 TeV and an integrated luminosity of 500 fb^{-1}. In (a) we display the results for a $e\gamma$ collider while (b) contains the results for the $\gamma\gamma$ mode.

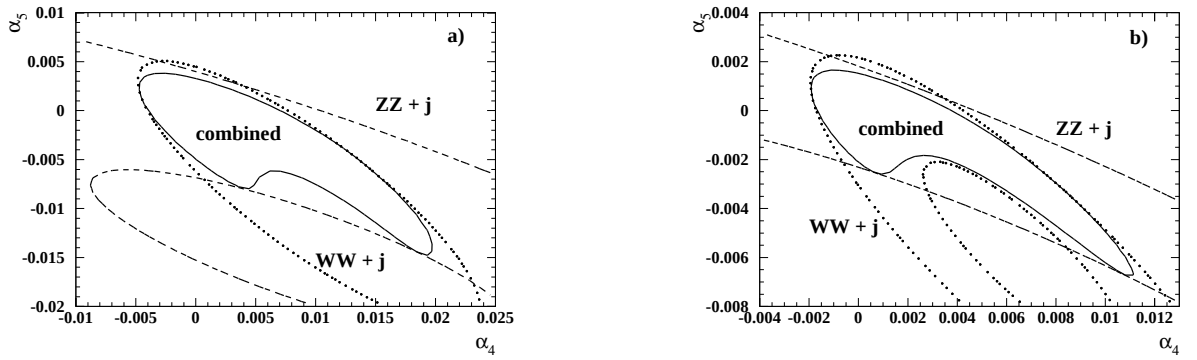

FIG. 4. 90% CL allowed region in the (α_4, α_5) plane assuming that we observed the number of events predict by the SM without a Higgs boson in the $e\gamma \to WW$ + jet (dots), $e\gamma \to ZZ$ + jet (dashes), and combined reactions (solid). We assumed a e^+e^- center–of–mass energy of 2 TeV (a) [3 TeV (b)] and an integrated luminosity of 500 fb^{-1}.

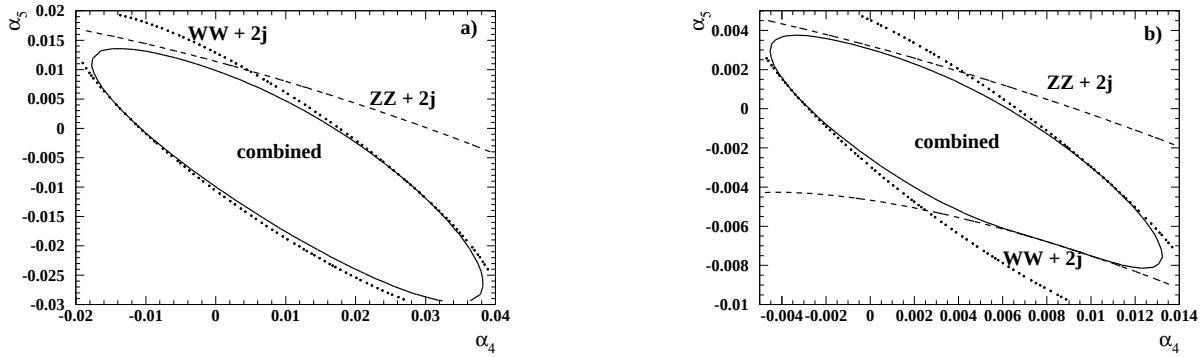

FIG. 5. 90% CL allowed region in the (α_4, α_5) plane assuming that we observed the number of events predict by the SM without a Higgs boson in the $\gamma\gamma \to WW$ + 2 jets (dots), $\gamma\gamma \to ZZ$ + 2 jets (dashes), and combined reactions (solid). We assumed a e^+e^- center–of–mass energy of 2 TeV (a) [3 TeV (b)] and an integrated luminosity of 500 fb^{-1}.

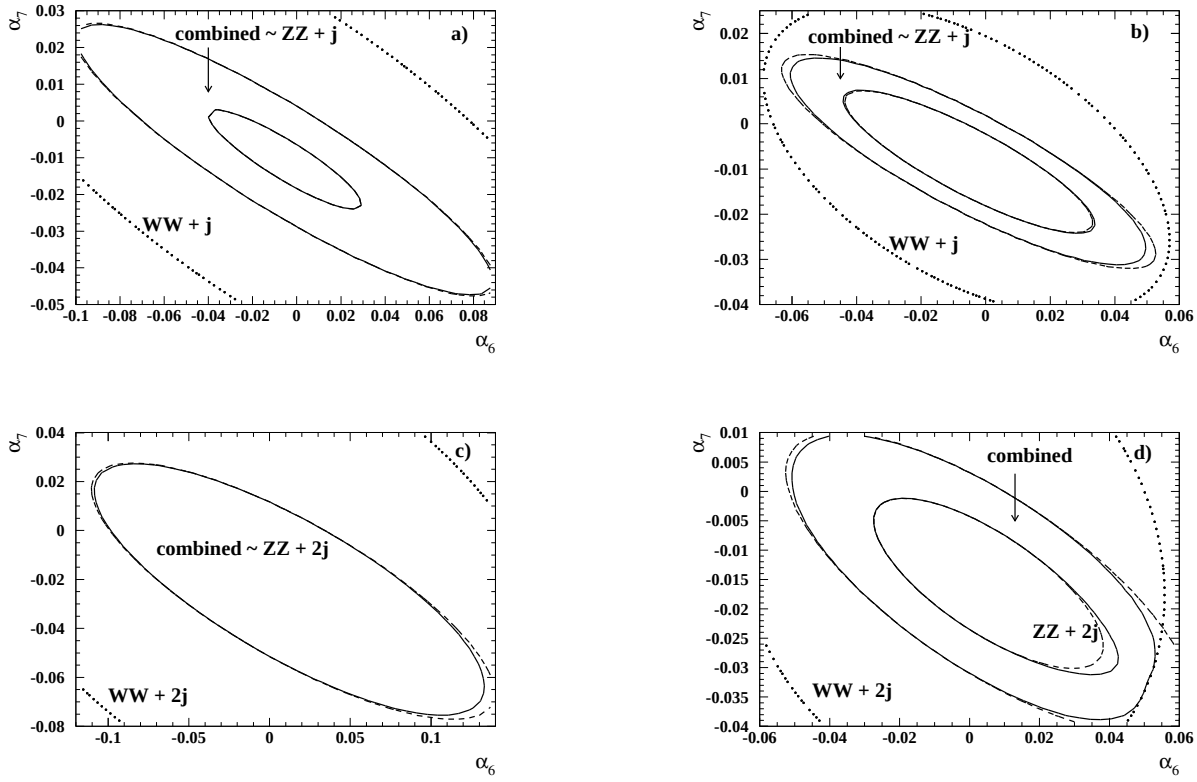

FIG. 6. Combined 90% CL allowed region in the (α_6, α_7) plane assuming that we observed the number of events predict by the SM without a Higgs boson in the $e\gamma$ mode [(a) and (b)] and $\gamma\gamma$ one [(c) and (d)]. We assumed a e^+e^- center–of–mass energy of 2 TeV in (a) and (c) and 3 TeV in (b) and (d), and an integrated luminosity of 500 fb^{-1}.